Control of targeting ligand display by pH-responsive polymers on gold nanoparticles mediates selective entry into cancer cells

C. Brazzale[a], F. Mastrotto[a,b], P. Moody[c], P.D. Watson[d], A. Balasso[a], A. Malfanti[a], G. Mantovani[b], P. Caliceti[a], C. Alexander[b], A. T. Jones[c], S. Salmaso[a†]

Selective targeting of cells for intracellular delivery of therapeutics represents a major challenge for pharmaceutical intervention in disease. Here we show pH-triggered receptor-mediated endocytosis of nanoparticles via surface ligand exposure. Gold nanoparticles were decorated with two polymers: a 2 kDa PEG with a terminal folate targeting ligand, and a di-block copolymer including a pH-responsive and a hydrophilic block. At the normal serum pH of 7.4, the pH-responsive block (apparent pKa of 7.1) displayed a hydrophilic extended conformation, shielding the PEG-folate ligands, which inhibited cellular uptake of the nanoparticles. Under pH conditions resembling those of the extracellular matrix around solid tumours (pH 6.5), protonation of the pH-responsive polymer triggered a coil-to-globule polymer chain contraction, exposing folate residues on the PEG chains. In line with this, endocytosis of folate-decorated polymer-coated gold nanoparticles in cancer cells overexpressing folate receptor was significantly increased at pH 6.5, compared with pH 7.4. Thus, the tumour acidic environment and high folate receptor expression was effectively exploited to activate cell binding and endocytosis of these nanoparticles. These data provide proof-of-concept for strategies enabling extracellular pH stimuli to selectively enhance cellular uptake of drug delivery vectors and their associated therapeutic cargo.

Introduction

Over the past few decades the exploitation of nanoscale carrier vehicles to improve the therapeutic efficacy of drugs has offered much promise for biomedical applications.[1, 2] Poor biopharmaceutical profiles of most anticancer drugs and their systemic toxicity have stimulated the development of novel strategies to provide site-specific delivery to tumours. [3] These approaches are aimed at preventing undesired off-target effects by prolonging, in the first instance, blood circulation time and increasing the drug deposition in the tumour. [4] The extended circulation of drug nanocarriers, achieved by tailoring their size and surface properties, has been shown also to affect significantly passive targeting to tumours. [5] This can be attributed, at least in part, to the enhanced permeability and retention (EPR) effect which has been observed in animals and more recently implicated in some human cancers.[6-8] However, by relying solely on this strategy, drug release from the carrier can be limited in the extracellular disease site, and the poor permeability through biological membranes of therapeutics, especially macromolecules such as proteins and nucleic acids, further reduces the extent of intracellular drug accumulation.[4] Carrier surface decoration with targeting moieties for biorecognition of antigens or up-regulated receptors on the tumour cell plasma membrane (*e.g.*, anti-transferrin receptor antibody, peptides for integrin binding, and receptors for small molecules such as folate and galactose) has been successfully exploited to enhance the intracellular access of drug delivery systems.[9-12] A prototype of a successful actively targeted nanocarrier is CALAA-01, a transferrin-bearing cyclodextrin-based polymeric nanoparticle, which has been shown to deliver specific siRNAs intracellularly to exert their antitumour effects.[13] However, pre-clinical studies have shown to date that the active targeting approach has had limited effects on the therapeutic performance of 'classical' nanomedicines such as liposomes.[14, 15] The lack of targeting in these cases has been ascribed to a variety of anatomical and physiological barriers that must be systematically and sequentially overcome before tumour localisation is achieved and cancer cell intracellular compartments are accessed. Recently, increasing understanding of the physio-pathology of solid tumours has stimulated the development of tailor-made micro-environmentally sensitive nanocarriers with enhanced biorecognition properties. [3] Indeed, the peculiar physiological features of tumours compared to normal tissues, namely the lower extracellular pH, higher temperature and altered patterns of the extracellular enzymatic pool, have been regarded as opportunities to generate "smart" nanocarriers. [16] These are designed to exploit synergistically temporal and local micro-environmental conditions to distribute selectively in the tumour tissue and be taken-up by cancer cells to reach the intracellular target. [17-21] This approach can maximise the efficacy of the therapeutic treatment and minimise drug side effects.[19, 22] Attempts have also been pursued to activate *in situ* the responsive systems by inducing environmental alterations with external focused stimuli including magnetic fields, heating, ultrasound and light. [19,21-24]

We have selected gold nanoparticles (AuNPs) as nanoscale constructs to prove the concept that drug delivery systems can be 'instructed' to operate sequential tasks that are crucial to target cancer cells. Moreover, AuNPs were chosen in this study as a model nanoparticle platform by virtue of their ease of synthesis and surface decoration, but we believe our results have more general implications in the design of colloidal vehicles. AuNPs have a variety of biomedical applications, for example, in imaging, diagnostics, drug delivery, and cell sensitisation by external physical stimuli such as NIR laser light, ultrasound and X-rays. [22-28] Furthermore, drug-coated gold nanoparticles have been recently demonstrated to reduce multidrug resistance (MDR) of anticancer drugs. [29-31]

[a.] *Department of Pharmaceutical and Pharmacological Sciences, University of Padova, via F. Marzolo 5, 35131 Padova – Italy.*
[b.] *School of Pharmacy, University of Nottingham, University Park, Nottingham, NG7 2RD, UK.*
[c.] *Cardiff School of Pharmacy and Pharmaceutical Sciences, Cardiff University, Cardiff CF10 3NB – Wales (UK).*
[d.] *School of Biosciences, Cardiff University, Cardiff CF10 3AX– Wales (UK).*
† E-mail: stefano.salmaso@unipd.it
Electronic Supplementary Information (ESI) available: [details of any supplementary information available should be included here]. See DOI: 10.1039/x0xx00000x

We show here that the delivery of ligand-decorated polymer-functionalised AuNPs to cancer cells can be enhanced by exploiting specific tumour-mimetic conditions, which in turn trigger conformational changes of polymers coating the AuNPs. This environmentally-controlled responsiveness of AuNPs leads to the site-selective exposure of recognition ligands that provide for active targeting of the AuNPs to specific cells. This platform, in addition to being a versatile colloidal model, could also be exploited as sensitising agent that responds to external stimuli with enhanced site-selectivity for cancer therapeutic treatment.

Experimental

Materials and equipment. Synthesis of lipoyl-[$(MCH)_{26}$-*b*-$(GMA)_{53}$], OG-lipoyl-[$(MCH)_{26}$-*b*-$(GMA)_{50}$], lipoyl-$(GMA)_{79}$, folate-PEG_{2kDa}-SH (FA-PEG_{2kDa}-SH), and Bodipy FL-PEG_{2kDa}-SH (Bdp-PEG_{2kDa}-SH), as well as production of naked AuNPs and characterisation of naked and polymer decorated AuNPs are described in the electronic supporting information (ESI).

Evaluation of AuNP-polymer conjugation efficiency. Particles were incubated with increasing [polymer]:[AuNP] feed molar ratios to assess the efficiency of conjugation. 5.0 mg mL^{-1} FA-PEG_{2kDa}-SH, a 0.50 mg mL^{-1} Bdp-PEG_{2kDa}-SH and a 10 mg mL^{-1} lipoyl-[$(MCH)_{26}$-*b*-$(GMA)_{53}$] aqueous stock solutions were prepared. Samples of 3 nM AuNP suspensions were incubated with increasing molar excess of each polymer solution. More specifically, 3 nM AuNP suspensions (15 mL each) were added each respectively of 1.1, 2.2, 4.4, 11, 22, 44, 66 and 132 µL of 5 mg mL^{-1} FA-PEG_{2kDa}-SH solution in order to achieve [polymer]:[AuNP] feed molar ratios of 50:1, 100:1, 200:1, 500:1, 1000:1, 2000:1, 3000:1 and 6000:1; 3 nM AuNP suspensions (15 mL) were added each respectively of 2.5, 5, 10, 20, 50, 100, 200, 300 and 400 µL of 1 mg mL^{-1} Bdp-PEG_{2kDa}-SH solution in order to achieve [polymer]:[AuNP] feed molar ratios of 25:1, 50:1, 100:1, 200:1, 500:1, 1000:1, 2000:1, 3000:1 and 6000:1; 3 nM AuNP suspensions (15 mL) were added each respectively of 3.5, 7, 14, 35, 70, 140, 210 and 420 µL of 10 mg mL^{-1} lipoyl-[$(MCH)_{26}$-*b*-$(GMA)_{53}$] solution in order to achieve [polymer]:[AuNP] feed molar ratios of 50:1, 100:1, 200:1, 500:1, 1000:1, 2000:1, 3000:1 and 6000:1. Each polymer/AuNP mixture was brought to a final volume of 15.5 mL with Milli-Q water and incubated under rotational stirring at room temperature overnight. Afterwards, nanoparticles were isolated by centrifugation at 19720 x g for 30 min. Supernatants containing non-bound polymers were lyophilised and redissolved in 150 µL of Milli-Q water and tested by Iodine assay and UV-Vis spectroscopy after dilution (10 mM phosphate buffer, 137 mM NaCl, at pH 7.4 - PBS) at 363 nm to quantify FA-PEG_{2kDa}-SH concentration, Iodine assay and UV-Vis spectroscopy (ethanol) at 503 nm to quantify Bdp-PEG_{2kDa}-SH concentration (Bodipy FL molar extinction coefficient in ethanol at $\lambda_{503\ nm}$ = 80,000 $M^{-1}cm^{-1}$, as reported by the manufacturer), and UV-Vis spectroscopy (0.02 N NaOH) at 300 nm to quantify lipoyl-[$(MCH)_{26}$-*b*-$(GMA)_{53}$ concentration. [32, 33]

Assembly of polymer-decorated AuNPs.

Folate-targeted pH-responsive AuNPs: in a vial, 11 µL of a 0.50 mg mL^{-1} FA-PEG_{2kDa}-SH solution (5.46 µg, 2.25 nmol) in water were mixed to 9 µL of a 50 µg mL^{-1} mPEG_{2kDa}-SH solution in water (0.45 µg, 0.22 nmol). The mixture was added to a freshly prepared 3 nM AuNP suspension (15 mL) to yield a 50:5:1 [FA-PEG_{2kDa}-SH]:[mPEG_{2kDa}-SH]:[AuNP] feed molar ratio. The AuNP suspension was incubated at room temperature under rotational stirring overnight in the dark. The particle suspension was centrifuged at 19720 x g for 30 min, the AuNP pellet was washed twice with Milli-Q water. The supernatants were pooled, lyophilised and redissolved in 150 µL of Milli-Q water and analysed by UV-Vis spectroscopy (PBS, pH 7.4) at 363 nm and by Iodine test at 535 nm to quantify the unbound FA-PEG_{2kDa}-SH. Then the AuNP pellet was resuspended in 15 mL of water and added of 21 µL of a 0.50 mg mL^{-1} Bdp-PEG_{2kDa}-SH solution to yield a 100:1 [Bdp-PEG_{2kDa}-SH]:[AuNP] feed molar ratio mixture. The suspension was left under rotational stirring overnight at room temperature in the dark. In order to recover the unbound Bdp-PEG_{2kDa}-SH and assess its conjugation degree to AuNPs, the particle suspension was centrifuged and washed as described above, then the supernatant was lyophilised, redissolved in Milli-Q water and analysed by UV-Vis spectroscopy (ethanol) at λ=503 nm. Afterwards, the particle pellet was resuspended in 15 mL of Milli-Q water. The AuNP sample was added of 278 µL of a lipoyl-[$(MCH)_{26}$-*b*-$(GMA)_{53}$] solution in 0.02 N NaOH (8 mg mL^{-1}) to yield a 3000:1 [lipoyl-[$(MCH)_{26}$-*b*-$(GMA)_{53}$]]:[AuNP] feed molar ratio and the mixture was stirred overnight at room temperature in the dark. The particles were isolated by centrifugation at 19720 x g for 30 min, washed with Milli-Q water and centrifuged as described above and the supernatant was lyophilised, redissolved in 150 µL of Milli-Q water and analysed by UV-Vis spectroscopy (0.02 N NaOH) at 300 nm to quantify the amount of unbound lipoyl-[$(MCH)_{26}$-*b*-$(GMA)_{53}$. A reference mixture was also prepared with the same ratios and concentrations of polymers without AuNPs. The decoration efficiencies were derived by difference of the UV-Vis absorbances between the reference samples and the unbound polymers found in the supernatants of the AuNP containing samples.

Non-targeted pH-responsive AuNPs: 9.9 µL of a freshly prepared 0.50 mg mL^{-1} of mPEG_{2kDa}-SH solution (4.95 µg, 2.47 nmol) was added to 15 mL of freshly prepared 3 nM AuNP suspension to yield a 55:1 [mPEG_{2kDa}-SH]:[AuNP] feed molar ratio. Particle suspension was centrifuged at 19720 x g for 30 min, particles were washed with Milli-Q water as described above and the lyophilised supernatant was analysed by Iodine assay as described above to quantify the unbound PEG. Particles were then fluorescently labelled with Bdp-PEG_{2kDa}-SH and decorated with of lipoyl-[$(MCH)_{26}$-*b*-$(GMA)_{53}$] using the same procedure described for folate-targeted pH-responsive AuNPs.

Folate-targeted non-pH-responsive AuNPs: gold nanoparticles were decorated with FA-PEG_{2kDa}-SH and Bdp-PEG_{2kDa}-SH as described for folate-targeted pH-responsive AuNPs. Afterwards, 178 µL of a 10 mg mL^{-1} solution of lipoyl-$(GMA)_{79}$ in Milli-Q water was added to 15 mL of freshly prepared 3 nM AuNP suspension in order to yield a 3000:1 [lipoyl-$(GMA)_{79}$]:[AuNP] feed molar ratio. The mixture was stirred overnight at room temperature in the dark. The un-bound lipoyl-$(GMA)_{79}$ was quantified by Iodine assay on the supernatant after particle centrifugation at 19720 x g for 30 min, lyophilisation and redissolution in 150 µL of Milli-Q water.

Cell culture and viability assay. MCF-7 (human breast adenocarcinoma) and KB (human cervical carcinoma) cells were grown and tested for particle toxicity according to previously reported protocols (ESI).[27]

Particle cell uptake by Atomic Absorption Spectroscopy. MCF-7 and KB cells were seeded in 12-well plates at a density of 5 x 10^5 cells per well and grown for 48 h. Then the medium was discharged, the cells were washed 3 times with PBS at pH 7.4 and incubated with 2 nM particle suspensions in FFDMEM at pH 7.4 and 6.5. After 2 h of incubation at 37 °C in 5% CO_2 atmosphere, the medium was removed and the cells were washed thrice with PBS. Cells were then detached by treatment with 1% (w/v) trypsin in PBS (150 µL/well). Trypsin was quenched by adding 500 µL of PBS containing

1 mM $CaCl_2$ and $MgCl_2$ and cell suspensions were centrifuged at 160 x g for 5 min. Cell pellets were washed twice with PBS containing 1 mM $CaCl_2$ and $MgCl_2$, then added of 0.1% Triton® X-100 in water (600 µL/sample) and treated with ultrasounds for 1 hr to induce lysis. Samples were centrifuged at 160 x g for 5 min. Cell lysates (500 µL) were digested by treatment with aqua regia (1:3 v/v HNO_3/HCl, 5 mL) at 80 °C for 1 hour. The mineralised sample volumes were brought to 5 mL with 1% (w/v) HCl. Gold quantification was performed by Atomic Absorption Spectrometry (AAS). Gold concentration in the samples was normalised by the number of cells which was derived from a standard curve made by BCA Protein Assay (Thermo Fisher Scientific Inc., Waltham, MA-USA) performed on 100 µL dilutions of cell lysate at known concentrations (cells/mL).

Flow cytometric analysis. KB cells were seeded in 12-well plates at a density of 3 x 10^5 cells per well and allowed to adhere and grow for 48 h under tissue culture conditions. The medium was replaced with 2 nM particle suspensions in FFDMEM at pH 7.4 or 6.5. Cells were incubated for 2 h at 37 °C in a humidified 5% CO_2 atmosphere and then washed thrice with 1 mL PBS and detached by 4 min treatment with 1% (w/v) trypsin in PBS (150 µL/well) at 37 °C. Trypsin activity was quenched by adding 500 µL of PBS containing 1 mM $CaCl_2$ and $MgCl_2$ and cells were recovered by centrifugation at 160 x g for 5 min. Cells were then fixed in freshly prepared 4% (w/v) paraformaldehyde (PFA) in PBS for 15 min at room temperature, centrifuged at 160 x g for 5 min, washed once with PBS and resuspended in 300 µL of PBS. The samples were analysed at λ_{ex}=488 nm, λ_{em}=525 nm using a BD FACSDiva flow cytometer (Becton, Dickinson and Company, Buccinasco, Milan) and the results were processed with BD FACSDiva Software. Cell competition assay was performed by incubating KB cells with particle suspensions in FFDMEM at pH 7.4 or 6.5 containing 200 µM folic acid. After 2 h incubation time, the samples were processed as described above.

Confocal microscopy. MCF-7 and KB cells were seeded onto 35 mm glass bottom dishes (MatTek, Ashland, US) at a seeding density of 1.5 x 10^5 cell per well in FFDMEM containing 15% FBS and grown for 48 h under tissue culture conditions. The medium was removed, cells were washed thrice with 1 mL of PBS and incubated with 2 nM particle suspensions in FFDMEM at pH 7.4 and 6.5 (250 µL/dish) at 37 °C in the dark for 2 h. Particle samples were then removed and wells were gently washed with PBS (1 mL x 3). Cells were incubated in pre-warmed imaging medium (phenol red-free DMEM pH 7.4 containing 25 mM HEPES and supplemented with 1 mg mL^{-1} BSA). Cells were imaged on a Leica TCS SP5 confocal laser-scanning microscope using 488 nm laser excitation of Bodipy FL.
Cell competition assay was performed by incubating KB cells with Folate-targeted pH-responsive AuNPs in FFDMEM for 2 h at pH 7.4 or 6.5 enriched of 200 µM folic acid. The samples were imaged and analysed as above.

Transmission electron microscopy (TEM). Intracellular disposition of AuNPs was imaged by TEM analysis. KB cells were seeded at the density of 3 x 10^5 cells per well in 12 well plates and allowed to adhere and grow for 48 h under tissue culture conditions. Cells were incubated with 2 nM particle suspensions in FFDMEM at pH 7.4 and 6.5 for 2 h at 37 °C. The incubation medium was removed and cells were washed thrice with 1 mL PBS and fixed with 2.5 % (w/v) glutaraldehyde in 0.1 M sodium cacodylate buffer at 4 ˚C for 1 hr. The cells were washed twice with sodium cacodylate buffer and post fixed in 0.1 M sodium cacodylate buffer containing 1% (w/v) osmium tetroxide for 1 hr, dehydrated using ethanol and embedded in fresh EPON resin. Ultrathin sections of the samples were cut and observed with a Tecnai G2 Transmission Electron Microscope (FEI, Oregon, USA).

Statistical analysis. All experiments were carried out three times and each sample was generated in triplicate. Data are presented as mean ± S.E calculated from three independent experiments. Statistical analyses were performed with GraphPad software. Statistical comparisons between treatment groups were performed with analysis of variance (one-way ANOVA) and the threshold of significance was calculated according to Bonferroni's test. Statistical significance was attained for values of $p<0.05$.

Results and discussion

This proof of concept study aimed to enhance the site-selectivity of nanoparticles to a tumour environment. The extracellular pH of many solid tumour tissues is typically in the 6-7 range, thus more acidic than most healthy tissues, due to modification of cancer cell energetic metabolism.[34, 35] The hypoxic condition is one of the major causes that drive tumour cells to metabolise glucose abnormally in the glycolytic pathway. Accordingly, the high production of lactic acid and proton pump activity lead to acidification of the tumour extracellular environment.[34, 36]
Our approach is aimed at exploiting this gradient of pH as an 'on/off' switch whereby functional ligands on NPs are hidden under conditions mimicking those found in systemic circulation, but which can be subsequently exposed in the more acidic tumour microenvironment, thus enhancing selectivity for specific cancer cells. With this purpose, pH-responsive polymers were chosen that would shield the surface of NPs at physiological pH, then shrink under more acidic conditions, revealing the ligands of choice (Figure 1). Accordingly, the study was carried out by using three main components: AuNPs, folic acid as model targeting agent and a pH-responsive di-block copolymer. A fluorescent tag, Bodipy FL, was also conjugated to the AuNPs as tracer for biological investigations.
AuNPs were chosen as model colloidal systems because they can be easily manufactured and then modified with multiple components through the formation of strong metal-sulfur bond.[37] Previous studies have shown that hydrophilic polymer-coated AuNPs with a core size of less than 20 nm exhibit prolonged blood half-life compared to larger particles, thus in this work AuNPs with an average diameter of 15 nm were used.[38] Folic acid is commonly used to selectively target cancer cells that overexpress the folate receptor; this promotes cell uptake through receptor mediated endocytosis.[39, 40] Finally, a pH-responsive block copolymer based on 3-chloro-4-hdroxybenzoic esters was used to generate AuNPs able to undergo surface structural changes induced by pH variations in the physio-pathological range of healthy and tumour tissue, set here at pH 7.4 and 6.5 respectively.[41-43]

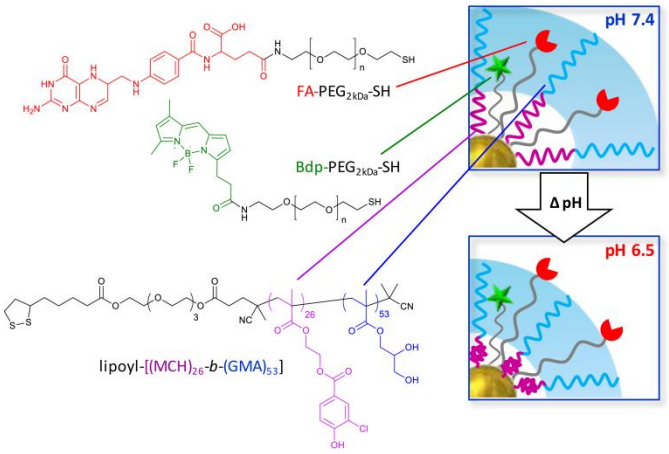

Figure 1. *Hide-and reveal* smart AuNPs. Left. Chemical structures of the three polymeric components used to assemble the nanosystem: FA-PEG_{2kDa}-SH, Bdp-PEG_{2kDa}-SH and lipoyl-$[(MCH)_{26}$-*b*-$(GMA)_{53}]$. Right. Schematic representation of the responsive AuNPs: at physiological pH (7.4) the responsive copolymer is in the extended conformation which masks the targeting agent FA-PEG_{2kDa}-SH; at acidic pH (6.5) of the tumour, lipoyl-$[(MCH)_{26}$-*b*-$(GMA)_{53}]$ collapses, which exposes the targeting agent that can bind the folate receptor and guide particle internalisation.

Synthesis of coating materials.

Folic acid was conjugated to the particle surface through a flexible PEG_{2kDa}-SH spacer which was calculated to have a fully extended chain length of 18 nm.[44] Notably, PEGylated liposomes currently used in the clinic (Doxil® and Caelyx®) are produced with a 2 kDa PEG corona to minimise vesicle opsonisation and complement activation that results in prolonged blood circulation time. [6, 45] Accordingly, folate-PEG_{2kDa}-SH (FA-PEG_{2kDa}-SH, Figure 1) with a ω-sulfhydryl group suitable for conjugation to AuNPs was synthesised by reacting *N*-hydroxysuccinimidyl-ester activated folic acid (FA-NHS) with NH_2-PEG_{2kDa}-SH using a 3:1 FA-NHS/NH_2-PEG_{2kDa}-SH molar ratio in order to maximise the PEG derivatisation (Scheme S1). After purification and treatment with TCEP to reduce the disulfide species formed during the synthesis of FA-PEG_{2kDa}-SH, a 96% chain-end fidelity in thiol groups was found. Structurally analogous green fluorescent Bdp-PEG_{2kDa}-SH (Figure 1), was synthesised to fluorescently tag AuNPs and facilitate their tracking during *in vitro* cell studies. Bdp-PEG_{2kDa}-SH (λ_{ex} 503 nm, λ_{em} 509 nm) was obtained by conjugating *N*-hydroxysuccinimidyl ester activated Bodipy FL (Bdp-NHS) to NH_2-PEG_{2kDa}-SH (Scheme S2). A 2 kDa PEG linker was chosen as previous studies showed that a spacers with a length longer than 6 nm, corresponding to an extended PEG chain with a molecular weight of 0.75 kDa, are needed to prevent fluorescence quenching induced by the gold surface.[46]

A novel Au-reactive lipoyl-poly[2-(methacryloyloxy)ethyl-3-chloro-4-hydroxybenzoate]-*b*-[glycerol methacrylate] (lipoyl-$[(MCH)_{26}$-*b*-$(GMA)_{53}]$) copolymer (Figure 1) was designed for this work to bestow AuNPs with pH induced surface conformational changes in the physio-pathological range of blood and tumour tissue. Notably, the 2-(methacryloyloxy)ethyl-3-chloro-4-hydroxybenzoate (MCH) monomer was selected by virtue of its substituted phenol group pKa with a value ~7. This is prevalently in its anionic hydrophilic state at pH 7.4, while it protonates and converts into a neutral hydrophobic form under acidic conditions.[42]

The length selection of each polymeric component used to coat the particles and the individual blocks of the responsive copolymer was key to allow the *hide-and-reveal* of the FA-PEG_{2kDa}-SH targeting agent. Accordingly, the pH-responsive lipoyl-$[(MCH)_{26}$-*b*-$(GMA)_{53}]$ copolymer with a calculated chain-extended length of 25.5 nm (10.7 nm length of the pH-responsive polyMCH block and 14.8 nm length of the hydrophilic non-responsive polyGMA block) was synthesised. At physiological pH, the two blocks were expected to be hydrophilic due to the presence of hydrated glycerol and ionised 3-chloro-4-hydroxybenzoate side-chains, and assume an extended conformation, allowing for the *shielding* of the shorter FA-PEG_{2kDa}-SH targeting agent (Figure 1, pH 7.4). We hypothesised that under the acidic conditions often found in solid tumour environments, protonation of the 3-chloro-4-hydroxybenzoate residues would cause the polyMCH block to become hydrophobic, inducing a transition of these polymer chains from extended coils to collapsed globule-like conformations on the AuNP surface (Figure 1, pH 6.5). In turn, this would result in an overall shortening of the lipoyl$[(MCH)_{26}$-*b*-$(GMA)_{53}]$ chains, and *unmasking* of the folate-targeting agents.

A lipoic ester chain-end was chosen because of its ability to form stable S-Au bonds, and to be inert under the radical polymerisation conditions utilised to prepare these copolymers.[47] Accordingly, lipoyl-$[(MCH)_{26}$-*b*-$(GMA)_{53}]$ was generated by RAFT polymerisation using a novel chain-transfer agent (CTA) that was designed to control the polymerisation process and introduce a lipoic acid moiety at the polymer α-chain end (Scheme 1A).

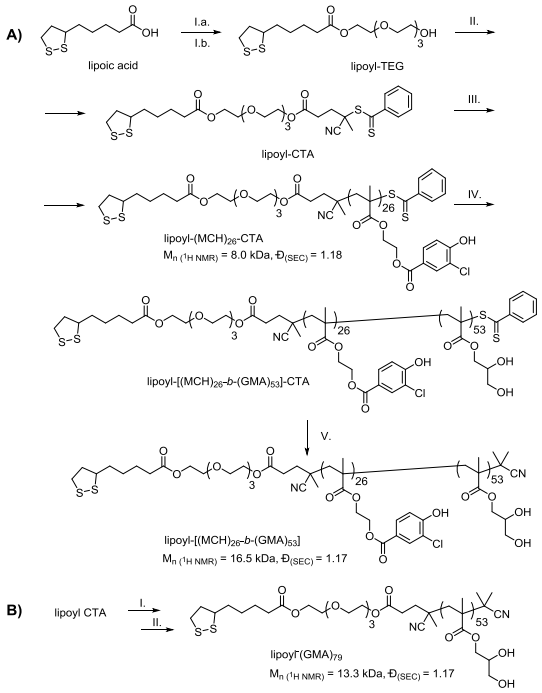

Scheme 1. (A) Synthesis of lipoyl-CTA. I.a. Oxalyl chloride, DCM 0 °C. I.b. TEG, Et_3N, DCM. II. 4-cyano-4-(phenylcarbonothioylthio) pentanoic acid/DCC/DMAP, DCM 0 °C. Synthesis of the lipoyl-$[(MCH)_{26}$-*b*-$(GMA)_{53}]$. III. MCH, AIBN, DMF 70 °C. IV. GMA, AIBN, DMF 70 °C. V. AIBN, DMF 70 °C. (B) Synthesis of the lipoyl-$(GMA)_{79}$.

Lipoic acid was first converted into its corresponding acid chloride with oxalyl chloride, then esterified with an excess of tetraethylene glycol (TEG) and finally conjugated to 4-cyano-4-(phenylcarbonothioylthio) pentanoic acid using DCC/DMAP to yield the desired lipoyl-CTA. The di-block copolymer lipoyl-$[(MCH)_{26}$-*b*-$(GMA)_{53}]$-CTA was synthesised by polymerisation of 2-(methacryloyloxy) ethyl-3-chloro-4-hydroxybenzoate monomer (MCH) in the presence of lipoyl-CTA and then utilising the resulting lipoyl-$(MCH)_{26}$-CTA as macro transfer agent for the subsequent polymerisation of hydrophilic glycerol methacrylate (GMA). Finally,

removal of the dithiobenzoic end groups from lipoyl-[$(MCH)_{26}$-*b*-$(GMA)_{53}$]-CTA was carried out according to the procedure developed by Perrier *et al*., using an excess of AIBN at 80 °C in DMF for 4 h and resulted in the disappearance of the pink colour from the isolated final polymer.[48, 49]

We have previously shown that the ability of polyMCH-based copolymers to undergo hydrophilic/hydrophobic switching depends on both polymer composition- i.e. chemical structure and relative molar ratio of the monomers and molecular weight of their individual blocks.[42] In particular, we found that a poly(MCH-*b*-GMA) copolymer with a degree of polymerisation of 80 and a MCH/GMA ratio of 1:2 underwent morphological rearrangement in the 7.4-6.5 pH range, required in the present study. Moreover, preliminary studies performed by exposing AuNPs decorated with poly(MCH-*b*-GMA) possessing a 1:2 MCH/GMA ratio to pH 7.4 and 6.5 showed the particle stability at both pH conditions. However, a higher MCH ratio in the polymer backbone led to AuNP aggregation at pH 6.5 which is undesirable for *in vitro/in vivo* applications.

A non-pH-responsive polymer, lipoyl-$(GMA)_{79}$, with the same total number of repeating units as lipoyl-[$(MCH)_{26}$-*b*-$(GMA)_{53}$] was synthesised to produce 'control' folate-targeted non-pH-responsive AuNPs (Scheme 1B).

pH-responsiveness of lipoyl-[$(MCH)_{26}$-*b*-$(GMA)_{53}$].

The pKa of the pH-responsive copolymer was determined by potentiometric acid/base titration and back titration. In agreement with previous reports, Figure 2A shows that, a decrease of pH induced reversible protonation of MCH repeating units.[42, 50] In turn, this prompted an increase of the hydrophobicity of the polyMCH block that resulted in reversible self-assembly.[42] This likely prevented access of the titrant to all phenolic groups of polyMCH, thus partially interfering with the titration process, hence the pKa 7.1 measured in these experiments is referred to here as "apparent pKa".

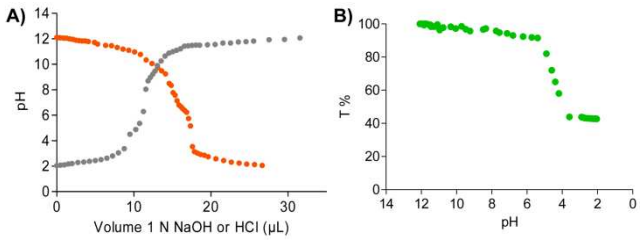

Figure 2. (A) Potentiometric Titration (●) and back titration (●) profiles of lipoyl-[$(MCH)_{26}$-*b*-$(GMA)_{53}$]. (B) Turbidimetric profile (●) of lipoyl-[$(MCH)_{26}$-*b*-$(GMA)_{53}$].

Turbidimetric analysis was performed to assess the polymer cloud point (CP) corresponding to its phase-separation in solution. CP is a descriptor of the material aggregation behaviour that stems from the increased hydrophobicity of the polyMCH as the pH decreases, which ultimately leads to formation of visible aggregates, which occurred at pH 5.2 (Figure 2B). The observed pKa and CP values of the copolymer were found to be in reasonable agreement with the estimated LogD values of MCH (LogD at pH 7.4 = 3.29; LogD at pH 6.5 = 3.71). This supported the increase in hydrophobicity of the pH-sensitive monomer as the pH decreases from pH 7.4 to 6.5.[51]

Thus, protonation of MCH monomers under acid conditions causes the polyMCH blocks of the pH responsive polymer to become more hydrophobic. It should be noted that the self-assembly process of the lipoyl-[$(MCH)_{26}$-*b*-$(GMA)_{53}$] is observed upon gradual acidification of aqueous solutions, where polymer chains are free to assemble into nanostructures (Supporting information, Table S1). However, at the surface of AuNPs the mobility of polymer chains is restricted due to their lipoic ester chain-end being chemically linked to the gold surface. As a result, chain-chain assembly should be prevented, and lowering of pH will result in an increase of the hydrophobicity of the individual polyMCH blocks, their dehydration, and consequent collapse to minimise contact area with water, thus exposing FA-PEG_{2kDa}-SH ligands via a *hide and reveal* mechanism.

Assembly and characterisation of folate-targeted pH-responsive AuNPs.

In order to set-up a suitable coating protocol, initial preliminary studies were carried out to assess the conjugation efficiency of each polymeric component to AuNPs.

The FA-PEG_{2kDa}-SH, Bdp-PEG_{2kDa}-SH and lipoyl-[$(MCH)_{26}$-*b*-$(GMA)_{53}$] coating efficiencies, defined as polymer chains/nm^2, were calculated by spectrophotometric quantification of the unbound polymers after conjugation to AuNPs. Figure 3A shows that the maximal densities of FA-PEG_{2kDa}-SH and Bdp-PEG_{2kDa}-SH on the gold surface were 1.2 polymer chain/nm^2 for both polymers in agreement with the density values reported in literature for PEG of comparable molecular weight.[52] [FA-PEG_{2kDa}-SH]:[AuNP] and [Bdp-PEG_{2kDa}-SH]:[AuNP] feed molar ratios below 200:1 in the coating process yielded over 90% of polymer conjugation. The maximal lipoyl-[$(MCH)_{26}$-*b*-$(GMA)_{53}$] density on the AuNP surface was 1.10 chains/nm^2, which was very similar to FA-PEG_{2kDa}-SH and Bdp-PEG_{2kDa}-SH. [Lipoyl-[$(MCH)_{26}$-*b*-$(GMA)_{53}$]]:[AuNP] feed molar ratios below 200:1 also yielded over 90% coating efficiency.

The folate-targeted pH-responsive AuNPs were then obtained following a three-step procedure: i) surface modification with FA-PEG_{2kDa}-SH, ii) fluorescent labelling with Bdp-PEG_{2kDa}-SH, iii) surface saturation with the pH-responsive copolymer lipoyl-[$(MCH)_{26}$-*b*-$(GMA)_{53}$].

In the first step, the particles were functionalised using a 50:1 [FA-PEG_{2kDa}-SH]:[AuNP] feed molar ratio. Our previous studies demonstrated that 18 nm AuNPs functionalised with 50 folate molecules/particle possessed high binding avidity to immobilized receptors and were efficiently internalised by KB cells overexpressing the folate receptor.[52] This degree of folate labelling was shown to promote the highest cell uptake of nanoparticles with respect to lower and higher densities, which was ascribed to multivalent clustering of folate receptors on cell.[53, 54]

However, the AuNP coating with FA-PEG_{2kDa}-SH was found to yield unstable particles that prevented their handling in subsequent derivatisation steps. This may be attributed to the hydrophobicity of folate. In order to overcome the stability problems, a 5:50 [mPEG_{2kDa}-SH]:[FA-PEG_{2kDa}-SH]:[AuNP] feed molar ratio mixture was used. In the second step, 100:1 [Bdp-PEG_{2kDa}-SH]:[AuNP] feed molar ratio was used to label the nanoparticles. Finally, in the third step the particle surface was saturated with the pH-responsive copolymer using a 3000:1 [lipoyl-[$(MCH)_{26}$-*b*-$(GMA)_{53}$]]:[AuNP] feed molar ratio.

Each coating step was followed by particle purification by centrifugation and spectrometric determination of the unbound polymers in the supernatant. Polymer conjugation efficiency was found to be 97%, 95% and 13% for FA-PEG_{2kDa}-SH, Bdp-PEG_{2kDa}-SH and lipoyl-[$(MCH)_{26}$-*b*-$(GMA)_{53}$], respectively, which corresponded to a mean of 48, 95 and 390 polymer chains per AuNP, respectively. The calculated total polymer density was 0.75 chains/nm^2, which is slightly lower than that obtained by the direct conjugation of the single polymers. This result suggests that the presence of polymers on the nanoparticle surface during the multi-step coating can hinder the subsequent insertion of further polymer chains thus limiting the final coating efficiency. The observed low lipoyl-[$(MCH)_{26}$-b-$(GMA)_{53}$] conjugation efficiency here is simply due to

the large excess of polymer used to maximise polymer density at the particle surface.

Control non-targeted pH-responsive AuNPs and control folate-targeted non-pH-responsive AuNPs were prepared following an analogous protocol, using mPEG$_{2kDa}$-SH instead of FA-PEG$_{2kDa}$-SH or by using lipoyl-(GMA)$_{79}$ instead of lipoyl-[(MCH)$_{26}$-*b*-(GMA)$_{53}$], respectively.

The concentration of the AuNP samples in suspension was calculated by UV-Vis analysis at λ=506 nm ($\varepsilon_{506\ nm}$ = 3.62 · 10^8 M^{-1} cm^{-1}, Figure 3B). Importantly, at this wavelength there is no appreciable absorption of FA-PEG$_{2kDa}$-SH and lipoyl-[(MCH)$_{26}$-*b*-(GMA)$_{53}$] and the absorption of Bdp-PEG$_{2kDa}$-SH is negligible ($\varepsilon_{506\ nm}$ = 80,000 M^{-1} cm^{-1}) compared to that of AuNPs.

Dynamic Light Scattering (DLS) and transmission electron microscopy (TEM) analyses were performed to characterise size and morphological features of both naked and polymer-decorated AuNPs. DLS size distributions (Figure 3E) showed that the size of AuNPs increased upon polymer conjugation, going from 14.5±1.6 to 34.2±3.1 nm for naked and folate-targeted pH-responsive AuNPs, respectively. Folate-targeted pH-responsive AuNPs maintained a narrow size distribution, with a polydispersity index (PDI) of 0.34±0.08. The control non-targeted pH-responsive particles and folate-targeted non-pH-responsive particles showed DLS profiles similar to the folate-targeted pH-responsive AuNPs, with a mean size of 31.4±4.2 and 35.3±2.6 nm, respectively (electronic supporting information, Figure S21).

TEM analysis showed that both naked and functionalised AuNPs had a spherical smooth shape (Figure 3C and 3D). Notably, the folate-targeted pH-responsive particles possess a grey corona surrounding the particle core further confirming the presence of a polymeric coating. TEM images elaboration of naked and folate-targeted pH-responsive AuNPs by ImageJ software showed mean sizes of 14.6±2.3 and 32.2±3.1 nm, respectively (Supporting information, Figure S22) which was in very good agreement with the DLS results.

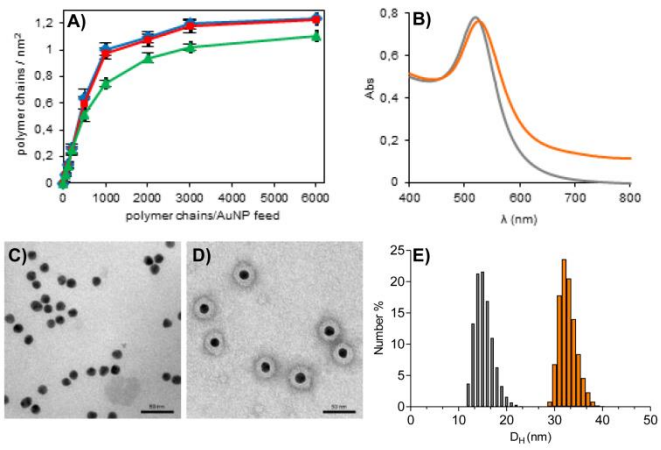

Figure 3. (A) Polymer density on particles surface at increasing [polymer]:[AuNP] feed molar ratio in the initial optimization experiments: FA-PEG$_{2kDa}$-SH (♦), poly(MCH-co-GMA) (▲), Bdp-PEG$_{2kDa}$-SH (■). (B) Absorption spectra of naked AuNPs (—) and folate-targeted pH-responsive AuNPs (—) in Milli-Q water. TEM images of (C) naked and (D) folate-targeted pH-responsive AuNPs in 10 mM PBS at pH 7.4. (E) DLS profile of naked AuNPs (■) and folate-targeted pH-responsive AuNPs (■) in 10 mM PBS at pH 7.4.

Particle stability studies were performed by incubating folate-targeted pH-responsive AuNPs in folate-free DMEM medium (FFDMEM) at pH 7.4 and 6.5. Sizes observed by DLS analyses of particle suspensions over a 4 h period were found to remain constant at both pH values. Interestingly, folate-targeted pH-responsive AuNPs showed a mean particle size of 38.2±3.8 nm and 53.2±11.5 nm at pH 7.4 and 6.5, respectively, which suggests that under acidic conditions MCH protonation in lipoyl-[(MCH)$_{26}$-*b*-(GMA)$_{53}$] may induce partial AuNPs self-aggregation. However, the presence of the polyGMA external corona was likely sufficient to ensure that even after collapse of the polyMCH blocks, colloidal stability of the polymer-functionalised AuNPs was maintained.

A dedicated assay was performed to investigate the morphological alterations of the pH-responsive polymer bound on the particle surface in response to pH changes. It is has been reported that substantial quenching of fluorescent molecules can take place when the dye is in the proximity of a metal nanoparticle surface.[55, 56] In particular, AuNPs with a size of 10-15 nm showed a massive loss in fluorescence when the distance of the fluorophore from the particle surface was below 6 nm.[46] Moreover, Acuna et al. clearly demonstrated that a decrease in the fluorescence signal could already be detected when the distance of the dye from the metal NPs surface was 14 nm, and that this was also negatively affecting the fluorophore lifetime. This phenomenon was exploited here to investigate polymer shrinkage at the surface of polymer-modified gold nanoparticles. A fluorescent pH-responsive polymer analogous to lipoyl-[(MCH)$_{26}$-*b*-(GMA)$_{53}$] was synthesised by including an oregon green methacrylate monomer (OGM) in the polyGMA hydrophilic block yielding OG-lipoyl-[(MCH)$_{26}$-*b*-(GMA)$_{50}$] (synthesis and characterisation are described in Supporting information). Oregon Green was chosen as fluorescent probe because of its lower pKa (typically in the 4.3-4.8 range) compared to other fluorescein-based dyes, which makes its fluorescence properties non pH-dependent, under the conditions utilised in this study (pH 6.5 and 7.4).[57] The incubation of the OG-lipoyl-[(MCH)$_{26}$-*b*-(GMA)$_{50}$] coated AuNPs at pH 6.5 induced a remarkable decrease of the particle fluorescence intensity, compared to that observed at pH 7.4, which was ascribed to the collapse of the polyMCH block causing the oregon green to get closer to the particle surface (Figure 4). Notably, the free OG-lipoyl-[(MCH)$_{26}$-*b*-(GMA)$_{50}$] in solution did not show fluorescence intensity alteration at pH 7.4 and 6.5 (Figure S18).

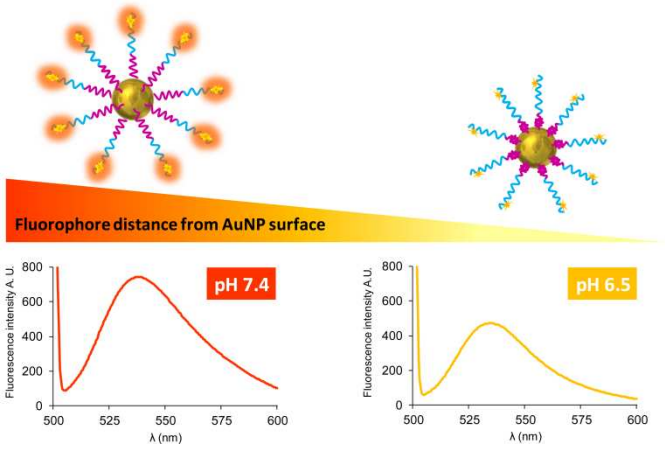

Figure 4. Fluorescence emission spectra of OG-lipoyl-[(MCH)$_{26}$-*b*-(GMA)$_{50}$] coated AuNPs at pH 7.4 (left) and 6.5 (right). Excitation wavelength was set at 496 nm. The top figure illustrates the morphological rearrangement of the polymer on the particle surface upon acidification from pH 7.4 to 6.5, and the resulting Oregon green fluorescence quenching.

In vitro biological studies

Cell viability

Cell viability studies were performed using MCF-7 human breast cancer and KB human cervical carcinoma cell lines to evaluate the cytocompatibility of the folate-targeted pH-responsive AuNPs at pH 7.4 and 6.5 (Figure 5). These two cell lines represent, respectively, low (lowFR) and high (hiFR) expressing folate receptor in *in vitro* models.[58] In both cell lines, cell metabolic activity (as a proxy for viability) after 24 h incubations was >85% at the two pH values for all selected folate-targeted pH-responsive AuNP concentrations utilised (0.2-2 nM).

Similar results were obtained with the control non-targeted pH-responsive (with $mPEG_{2kDa}$-SH instead of FA-PEG_{2kDa}-SH), and folate-targeted non-pH-responsive (lipoyl-$(GMA)_{79}$ instead of lipoyl-$[(MCH)_{26}$-*b*-$(GMA)_{53}]$ AuNPs (electronic supporting information, Figure S24).

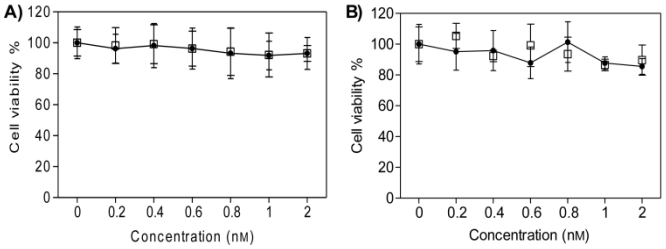

Figure 5. Cell viability profile of KB (A) and MCF-7 (B) cells incubated with increasing concentration of folate-targeted pH-responsive AuNPs at pH 7.4 (□) and 6.5 (◆) for 24 h.

Environmentally controlled cell uptake of particles

The assay was performed by incubating KB and MCF-7 cells with 2 nM functional AuNPs for 2 h. AuNP cell uptake was investigated by atomic absorption spectrometry, flow cytometry, confocal microscopy and transmission electron microscopy.

Atomic absorption spectrometry. Results showed that at pH 6.5 the uptake of the folate-targeted pH-responsive AuNPs in KB cells was ~3-fold higher than at pH 7.4 (Figure 6). The particle association with this cell line (8926 AuNPs /cell) was analogous to that found in previous studies where AuNPs decorated with folate-cysteamine were utilised.[52] The pH dependent cell uptake supports the hypothesis that at physiological pH (7.4) the lipoyl-$[(MCH)_{26}$-*b*-$(GMA)_{53}]$ is hydrophilic with an extended conformation that confers "stealth" properties to the nanosystem and hides the folate ligand from binding to the folate receptor. At acidic conditions, the increased polyMCH block hydrophobicity due to the protonation of the phenolic hydroxyl groups induces the pH-responsive block collapse on the particle surface resulting in copolymer shortening and consequent exposure of the targeting agent. The zeta potential of folate-targeted pH-responsive AuNPs and non-targeted pH-responsive AuNPs was -5.8 and -2.7 mV at pH 7.4 and -1.9 and -1.1 mV at pH 6.5, respectively. The slight decrease of zeta potential at pH 6.5 did not translate in the association of the control non-targeted pH-responsive AuNPs neither to KB nor MCF-7 cells, which proved that the association to KB cells is not driven by the limited decrease of the absolute value of particle zeta potential occurring when the polyMCH block of lipoyl-$[(MCH)_{26}$-b-$(GMA)_{53}]$ is increasingly neutralised. In MCF-7 cells, negligible AuNP uptake was observed at both pHs confirming that the AuNP internalisation was mediated by folate receptor recognition that takes place only when the pH-responsive polymer collapses. Crucially, incubation of control particles, non-targeted pH-responsive, and targeted non-pH-responsive AuNPs, did not show any appreciable uptake, further confirming that the observed AuNPs uptake was mediated by the folate receptor. Lipoyl-$(GMA)_{79}$ is expected to have the same chain length of lipoyl-$[(MCH)_{26}$-*b*-$(GMA)_{53}]$ but, lacking pH-responsive repeating units, it remains in its extended conformation at all pH values tested, thus efficiently masking the particle folate ligands. Notably, the results obtained with folate-targeted AuNPs decorated with non-responsive polymer lipoyl-$(GMA)_{79}$ confirmed that for the AuNPs investigated, *hide and reveal* mechanism was crucial to achieve efficient cell uptake.

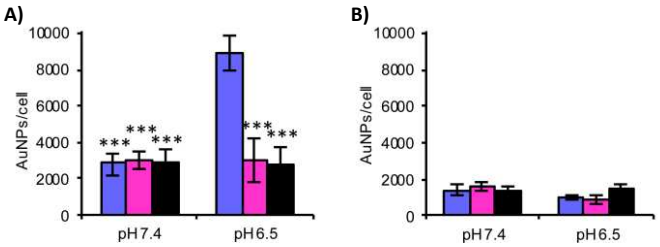

Figure 6. Cell uptake of folate-targeted pH-responsive AuNPs (■), non-targeted pH-responsive AuNPs (■) and folate-targeted non-pH-responsive AuNPs (■) at pH 7.4 and pH 6.5 by KB cells (A) and MCF-7 cells (B). Particles/cell was quantified by atomic absorption spectrometry on cell lysates. Statistical significance was calculated versus folate-targeted pH-responsive AuNP uptake at pH 6.5: *** p<0.001.

Flow cytometry. Cell uptake profile of polymer-decorated AuNPs was also investigated by flow cytometric analysis. Whilst not providing the absolute number of AuNPs internalised with each cell, this technique allowed comparison of the relative uptake of the different functional AuNPs. Figure 7 shows the association of non-targeted pH-responsive AuNPs, folate-targeted non-pH-responsive gold nanoparticles and folate-targeted pH-responsive gold nanoparticles at pH 7.4 and 6.5.

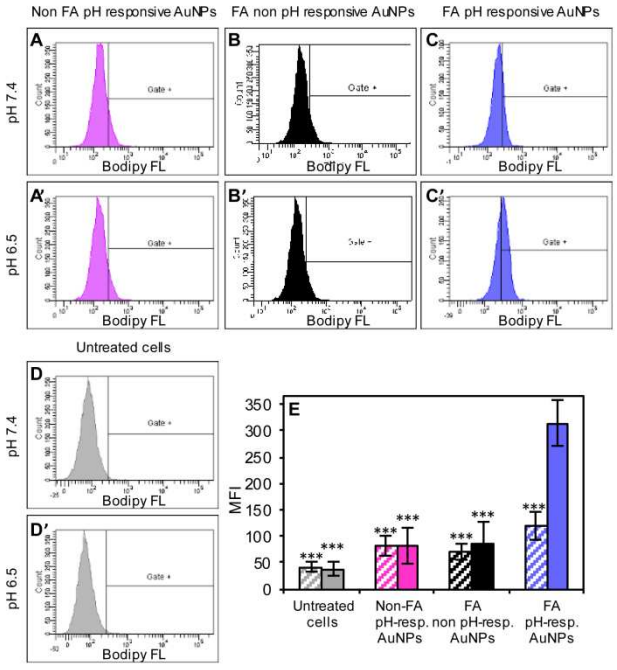

Figure 7. Flow cytometric profile at pH 7.4 (A-D) and 6.5 (A'-D') and mean fluorescence intensity (MFI) of KB cells (E) incubated with non-targeted pH-responsive AuNPs (Non-FA pH-resp. AuNPs), folate-targeted non-pH-responsive AuNPs (FA non-pH-resp. AuNPs) and folate-targeted pH-responsive AuNPs (FA pH-resp. AuNPs) at pH 7.4 (striped bars) and 6.5 (solid bars). Statistical significance was calculated versus folate-targeted pH-responsive AuNPs at pH 6.5: *** p<0.001.

Again, significant uptake was observed only for folate-targeted pH-responsive AuNPs at pH 6.5, in complete agreement with the results obtained in the atomic absorption spectroscopy experiments.

Confocal microscopy and TEM imaging. Confocal microscopic images of live cells Figure 8 showed that folate-targeted pH-responsive AuNPs were selectively and efficiently taken up by KB cells at pH 6.5, while at pH 7.4 very little cell-associated fluorescence was observed. In contrast, control non-targeted pH-responsive AuNPs underwent a much lower level of internalisation, again confirming the need for appropriate display of folate ligands to achieve efficient endocytosis. In an analogous manner, control folate-targeted non-pH-responsive AuNPs showed negligible cell association at both pH values, further confirming that lipoyl-$(GMA)_{79}$ coating could effectively mask the folate ligands on the particles. Importantly, the confocal images taken at the midpoint of the cells also revealed that the targeted particles were internalised by cells rather than confined on the cell membrane (electronic supporting information, Figure S25).

KB cells were also incubated with folate-targeted pH-responsive AuNPs in the presence of folic acid to assess specificity (Figure 8). Successful competition and thus reduced AuNP uptake was clearly detected when KB cells were incubated with folate-targeted pH-responsive AuNPs in the presence of folic acid at pH 6.5. This study further confirms that the folate-targeted pH-responsive AuNPs uptake is mediated by the specific binding of the exposed folate ligand of particles to the cell receptor. However, at pH 7.4 only a weak fluorescence was observed, which was further decreased in the presence of the competing free folic acid**.** This suggests that the limited particle uptake at pH 7.4 may be in part due to a residual specific binding to the folate receptor.

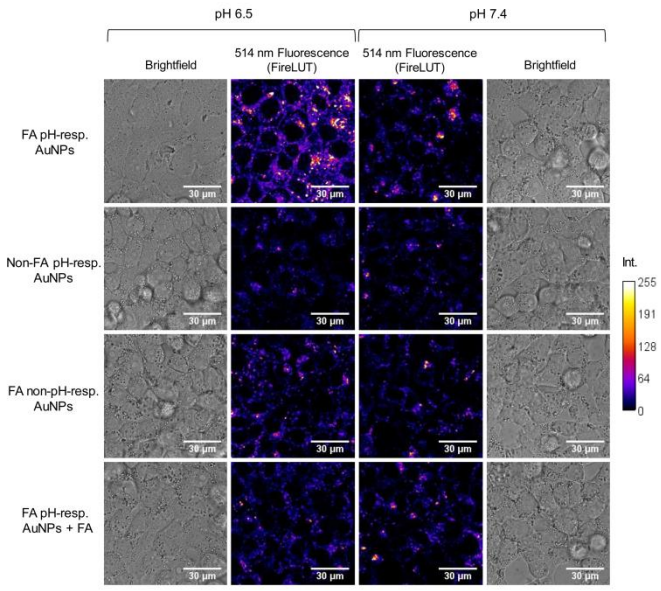

Figure 8. Confocal microscopic images of KB cells incubated with folate-targeted pH-responsive AuNPs (FA pH-resp. AuNPs), non-targeted pH-responsive AuNPs (Non-FA pH-resp. AuNPs), folate-targeted non-pH-responsive AuNPs (FA non-pH-resp. AuNPs) and FA pH-resp. AuNPs in the presence of 200 µM competing folic acid (FA pH-resp. AuNPs + FA) at pH 6.5 and 7.4. Fire LUT using ImageJ software was applied to the confocal images to visualize pixel intensity. Scale bars: 30 µm.

Transmission electron microscopy (TEM). Finally, ultrastructural disposition of AuNPs was investigated by TEM imaging of KB cells. Figure 9A and 9B show that at pH 6.5 the folate-targeted pH-responsive AuNPs were clearly visible inside KB cells.

Notably, the folate-targeted pH-responsive AuNPs are localised in membrane-limited intracellular compartments with no evidence of major aggregation, demonstrating that the hydrophilic and flexible polyGMA outer corona inhibited the particle aggregation.

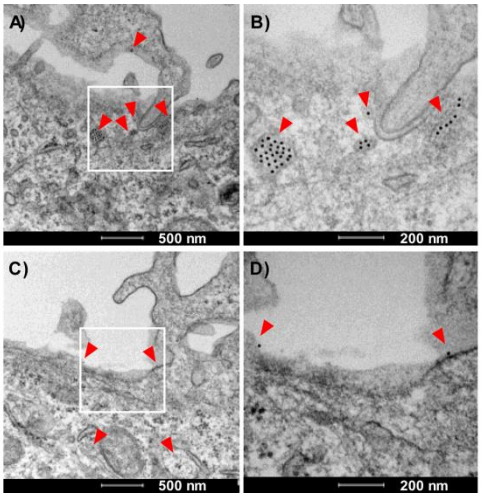

Figure 9. TEM images of folate-targeted pH-responsive AuNPs incubated with KB cells at pH 6.5 (A) and pH 7.4 (C). Red arrowheads point at AuNPs. Panel B and D are magnifications of the white squares in panel A and C, respectively.

Cells incubated with the folate-targeted pH-responsive AuNPs at pH 7.4, however, showed very little evidence of uptake although some particles could still be observed on the plasma membrane (Figure 9C and 9D). This low level of binding with no apparent uptake may account for the cell-associated particles detected under these conditions by atomic absorption spectroscopy and flow cytometric analyses at pH 7.4.

Conclusions

This proof-of-principle study shows that colloidal systems with dynamic surfaces can enhance site-selectivity for targeting cancer cells with high expression of plasma membrane receptors. Accordingly, these results suggest that physio-pathologic conditions of the extracellular tumour environment and cancer cell plasma membrane signature can be synergistically exploited to drive nanoparticle targeting and internalisation.

Importantly, the present work suggests that by finely programming the dynamic surface properties of nanosystems, site-selectivity can be significantly enhanced, thus reducing the disposition of drug nanocarriers and their often toxic payloads to off-target tissues. The tumour acidity-triggered 'hide and reveal' concept explored has potential for translation to a variety of colloidal carriers in a number of cancer settings.

Acknowledgements

We thank NanoSciERA (grant N° B51J09000200005), the EACEA Erasmus Programme and the Engineering and Physical Sciences Research Council (EPSRC Grants EP/J021180/1, EP/H005625/1 and EP/H006915/1) for funding this work. We acknowledge the University of Padova for financial support through the "Progetto di Ricerca di Ateneo" (grant N° CPDA121714; CUP C94H12000020005), "Progetto strategico di ateneo (Bando 2011" C98C13002740005, PROT. STPD11RYPT_02) and Ex-60% funding schemes. CB was recipient of a junior post-doctoral research fellowship granted by University of Padova (grant N° CPDR150704). We gratefully acknowledge Paul Cooling, Esme Ireson, Tom Booth, Christine

Grainger-Boultby, Jennifer Wymant, Edward Sayers and Michela Paccagnella for technical assistance.

References

1. J. Cheng and S. H. Pun, *Biomaterials Science*, 2015, DOI: 10.1039/C5BM90025E.
2. Z. X. Yang, S. G. Kang and R. H. Zhou, *Nanoscale*, 2014, **6**, 663-677.
3. T. Thambi, J. H. Park and D. S. Lee, *Biomaterials Science*, 2016, **4**, 55-69.
4. V. P. Torchilin, *The AAPS Journal*, 2007, **9**, E128-E147.
5. C. M. J. Hu, R. H. Fang, B. T. Luk and L. F. Zhang, *Nanoscale*, 2014, **6**, 65-75.
6. S. Salmaso and P. Caliceti, *Journal of Drug Delivery*, 2013, **2013**, 19.
7. Y. Matsumura and H. Maeda, *Cancer Research*, 1986, **46**, 6387-6392.
8. A. J. Clark, D. T. Wiley, J. E. Zuckerman, P. Webster, J. Chao, J. Lin, Y. Yen and M. E. Davis, *Proceedings of the National Academy of Sciences*, 2016, **113**, 3850-3854.
9. I. Cabezón, G. Manich, R. Martín-Venegas, A. Camins, C. Pelegrí and J. Vilaplana, *Molecular pharmaceutics*, 2015, **12**, 4137-4145.
10. C. Sarisozen, S. Dhokai, E. G. Tsikudo, E. Luther, I. M. Rachman and V. P. Torchilin, *Eur. J. Pharm. Biopharm.*, 2016, **108**, 54-67.
11. F. Danhier, A. L. Breton and V. r. Préat, *Molecular pharmaceutics*, 2012, **9**, 2961-2973.
12. A. Scomparin, S. Salmaso, A. Eldar-Boock, D. Ben-Shushan, S. Ferber, G. Tiram, H. Shmeeda, N. Landa-Rouben, J. Leor, P. Caliceti, A. Gabizon and R. Satchi-Fainaro, *Journal of Controlled Release*, 2015, **208**, 106-120.
13. J. E. Zuckerman, I. Gritli, A. Tolcher, J. D. Heidel, D. Lim, R. Morgan, B. Chmielowski, A. Ribas, M. E. Davis and Y. Yen, *Proceedings of the National Academy of Sciences*, 2014, **111**, 11449-11454.
14. A. Koshkaryev, R. Sawant, M. Deshpande and V. Torchilin, *Advanced Drug Delivery Reviews*, 2013, **65**, 24-35.
15. T. M. Allen and P. R. Cullis, *Advanced Drug Delivery Reviews*, 2013, **65**, 36-48.
16. C. Wang, X. Chen, X. Yao, L. Chen and X. Chen, *Biomaterials Science*, 2016, **4**, 104-114.
17. T. Tagami, W. D. Foltz, M. J. Ernsting, C. M. Lee, I. F. Tannock, J. P. May and S.-D. Li, *Biomaterials*, 2011, **32**, 6570-6578.
18. S. Mura, J. Nicolas and P. Couvreur, *Nature materials*, 2013, **12**, 991-1003.
19. R. M. Sawant, J. P. Hurley, S. Salmaso, A. Kale, E. Tolcheva, T. S. Levchenko and V. P. Torchilin, *Bioconjugate Chemistry*, 2006, **17**, 943-949.
20. L. Zhu, P. Kate and V. P. Torchilin, *ACS nano*, 2012, **6**, 3491-3498.
21. M. T. Basel, T. B. Shrestha, D. L. Troyer and S. H. Bossmann, *ACS nano*, 2011, **5**, 2162-2175.
22. J. V. Jokerst and S. S. Gambhir, *Accounts of chemical research*, 2011, **44**, 1050-1060.
23. W. Zhou, X. Gao, D. Liu and X. Chen, *Chem. Rev.*, 2015, **115**, 10575-10636.
24. J. Bhattacharyya, J. J. Bellucci, I. Weitzhandler, J. R. McDaniel, I. Spasojevic, X. Li, C.-C. Lin, J.-T. A. Chi and A. Chilkoti, *Nature communications*, 2015, **6**.
25. E. C. Dreaden, S. C. Mwakwari, Q. H. Sodji, A. K. Oyelere and M. A. El-Sayed, *Bioconjug. Chem.*, 2009, **20**, 2247-2253.
26. R. Robinson, W. Gerlach and H. Ghandehari, *J. Controlled Release*, 2015, **220**, 245-252.
27. C. R. Brazzale C, Foglietta F, Racca L, Durando G, Fantozzi R, Caliceti P, Salmaso S, Serpe L., *Nanomedicine*, 2016, **12**, 3053-3070.
28. D. B. Chithrani, S. Jelveh, F. Jalali, M. van Prooijen, C. Allen, R. G. Bristow, R. P. Hill and D. A. Jaffray, *Radiation research*, 2010, **173**, 719-728.
29. P. P. Constantinides and K. M. Wasan, *J. Pharm. Sci.*, 2007, **96**, 235-248.
30. F. Wang, Y.-C. Wang, S. Dou, M.-H. Xiong, T.-M. Sun and J. Wang, *ACS nano*, 2011, **5**, 3679-3692.
31. X. Zhang, H. Chibli, R. Mielke and J. Nadeau, *Bioconjug. Chem.*, 2011, **22**, 235-243.
32. G. E. C. Sims and T. J. Snape, *Anal. Biochem.*, 1980, **107**, 60-63.
33. D. M. Kranz, T. A. Patrick, K. E. Brigle, M. J. Spinella and E. J. Roy, *Proceedings of the National Academy of Sciences*, 1995, **92**, 9057-9061.
34. R. van Sluis, Z. M. Bhujwalla, N. Raghunand, P. Ballesteros, J. Alvarez, S. Cerdán, J.-P. Galons and R. J. Gillies, *Magn. Reson. Med.*, 1999, **41**, 743-750.
35. J. Griffiths, *Br. J. Cancer*, 1991, **64**, 425.
36. Y. Kato, S. Ozawa, C. Miyamoto, Y. Maehata, A. Suzuki, T. Maeda and Y. Baba, *Cancer Cell International*, 2013, **13**, 89-89.
37. L. Zhao, D. Jiang, Y. Cai, X. Ji, R. Xie and W. Yang, *Nanoscale*, 2012, **4**, 5071-5076.
38. S. D. Perrault, C. Walkey, T. Jennings, H. C. Fischer and W. C. W. Chan, *Nano Letters*, 2009, **9**, 1909-1915.
39. C. M. Paulos, J. A. Reddy, C. P. Leamon, M. J. Turk and P. S. Low, *Mol. Pharmacol.*, 2004, **66**, 1406-1414.
40. J. Sudimack and R. J. Lee, *Advanced drug delivery reviews*, 2000, **41**, 147-162.
41. F. Mastrotto, S. Salmaso, C. Alexander, G. Mantovani and P. Caliceti, *Journal of Materials Chemistry B*, 2013, **1**, 5335-5346.
42. F. Mastrotto, S. Salmaso, Y. L. Lee, C. Alexander, P. Caliceti and G. Mantovani, *Polymer Chemistry*, 2013, **4**, 4375-4385.
43. F. Mastrotto, A. F. Breen, G. Sicilia, S. Murdan, A. D. Johnstone, G. E. Marsh, C. Grainger-Boultby, N. A. Russell, C. Alexander and G. Mantovani, *Polymer Chemistry*, 2016, **7**, 6714-6724.
44. CambridgeSoft, ChemBio3D Ultra 12.0 software, 100 CambridgePark Drive, Cambridge, MA 02140, www.cambridgesoft.com.
45. M. Xing, F. Yan, S. Yu and P. Shen, *PloS one*, 2015, **10**, e0133569.
46. L. Rodriguez-Lorenzo, K. Fytianos, F. Blank, C. von Garnier, B. Rothen-Rutishauser and A. Petri-Fink, *Small (Weinheim an der Bergstrasse, Germany)*, 2014, **10**, 1341-1350.

47. J. M. Abad, S. F. Mertens, M. Pita, V. M. Fernández and D. J. Schiffrin, *J. Am. Chem. Soc.*, 2005, **127**, 5689-5694.
48. S. Perrier, P. Takolpuckdee and C. A. Mars, *Macromolecules*, 2005, **38**, 2033-2036.
49. H. Willcock and R. K. O'Reilly, *Polymer Chemistry*, 2010, **1**, 149-157.
50. E. Ravazzolo, S. Salmaso, F. Mastrotto, S. Bersani, E. Gallon and P. Caliceti, *Eur. J. Pharm. Biopharm.*, 2013, **83**, 346-357.
51. ChemAxon, MarvinSketch program, Budapest, Hungary.
52. F. Mastrotto, P. Caliceti, V. Amendola, S. Bersani, J. P. Magnusson, M. Meneghetti, G. Mantovani, C. Alexander and S. Salmaso, *Chemical communications*, 2011, **47**, 9846-9848.
53. C. Dalal, A. Saha and N. R. Jana, *The Journal of Physical Chemistry C*, 2016, **120**, 6778-6786.
54. S. Sabharanjak and S. Mayor, *Advanced drug delivery reviews*, 2004, **56**, 1099-1109.
55. G. P. Acuna, M. Bucher, I. H. Stein, C. Steinhauer, A. Kuzyk, P. Holzmeister, R. Schreiber, A. Moroz, F. D. Stefani and T. Liedl, *ACS nano*, 2012, **6**, 3189-3195.
56. G. Tan, K. Kantner, Q. Zhang, M. G. Soliman, P. del Pino, W. J. Parak, M. A. Onur, D. Valdeperez, J. Rejman and B. Pelaz, *Nanomaterials*, 2015, **5**, 1297-1316.
57. W.-C. Sun, K. R. Gee, D. H. Klaubert and R. P. Haugland, *The Journal of Organic Chemistry*, 1997, **62**, 6469-6475.
58. E. Gallon, T. Matini, L. Sasso, G. Mantovani, A. Armiñan de Benito, J. Sanchis, P. Caliceti, C. Alexander, M. J. Vicent and S. Salmaso, *Biomacromolecules*, 2015, **16**, 1924-1937.